Linear and Nonlinear Pressure Coupled Combustion Instability of Solid Propellants

R. S. Brown* and R. J. Muzzy†
United Technology Center, Sunnyvale, Calif.

A study has been made to relate theoretically predicted and experimentally observed pressure-coupled combustion instability behavior of solid propellants. Using a generalized theoretical model the linear and nonlinear region has been characterized by generalized combustion parameters. A comparison of the experimental data with theoretical predictions in the linear region (i.e., acoustic response functions) shows that small changes in propellant formulations can have a significant effect on the derived parameters characterizing the combustion. Analysis of the data shows that propellants having 84% solids loading are more likely to show the surface gasification to be pressure dependent than those having lower loadings; the temperature dependence of the gasification process is larger than can be explained by an Arrhenius rate expression with a reasonable activation energy; and the rate of energy transfer into the solid phase was found to increase with increasing surface temperature. This suggests the influence of exothermic surface processes. The effect of pressure on the energy transfer was found to be consistent with the several proposed models for gas-phase combustion effects. Higher order effects show that both positive and negative shifts in the time average burning rate with acoustic pressure can be obtained. Since Eisel has observed this effect to be negative, this defines the region of reasonable second order coefficients. Additional studies show that the acoustic response function can decrease with increasing acoustic pressure. Hence, the combustion process itself can limit the acoustic pressure amplitude in the T-burner.

Nomenclature

A_1 = $[\partial H_n/\partial\theta]_0$
A_2 = $[\partial^2 H_n/\partial\theta^2]_0$
A_3 = $[\partial^3 H_n/\partial\theta^3]_0$
B_1 = $[\partial F_n/\partial\epsilon]_0$
B_2 = $[\partial^2 F_n/\partial\epsilon^2]_0$
B_3 = $[\partial^3 F_n/\partial\epsilon^3]_0$
c = sonic velocity
c_p = specific heat
C_{11} = $[\partial^2 H_n/\partial\epsilon\partial\theta]_0$
C_{12} = $[\partial^3 H_n/\partial\epsilon\partial\theta^2]_0$
C_{21} = $[\partial^3 H_n/\partial\epsilon^2\partial\theta]_0$
D_{11} = $[\partial^2 F_n/\partial\theta\partial\epsilon]_0$
D_{12} = $[\partial^3 F_n/\partial\epsilon\partial\theta^2]_0$
D_{21} = $[\partial^3 F_n/\partial\epsilon^2\partial\theta]_0$
$E(\lambda)$ = $Re(\mu_2/\epsilon_1^2)$
E_2 = activation energy of over-all pyrolysis rate at surface
f_g, f_d = frequency of the acoustic pressure oscillations at the point where α_g and α_d measured
F = instantaneous heat flux into solid phase
F_n = F/F_0
F_0 = steady-state heat flux into solid phase = $\dot{r}_0\rho c_p(T_s^\circ - T_\infty)$
$F(\lambda)$ = $Re(\mu_3/\epsilon_1^3)$
G = gas temperature
H = rate of gasification at solid surface
H_n = $\dot{r}/\dot{r}_0$
$Im(\mu/\epsilon)$ = imaginary part of acoustic response function
J = burning rate in the gas phase
k = thermal conductivity
$\dot{m}_g$ = mass burning rate in the gas phase
$\dot{m}_s$ = mass flow rate from solid surface
n = steady-state burning rate exponent
n^1 = pressure exponent on surface pyrolysis
N = instantaneous flux into solid phase
P = instantaneous pressure
$\tilde{P}$ = amplitude of acoustic pressure oscillations
P_0 = steady-state pressure
Q_1 = $[\partial H_n/\partial\epsilon]_0$
Q_2 = $[\partial^2 H_n/\partial\epsilon^2]_0$
Q_3 = $[\partial^3 H_n/\partial\epsilon^3]_0$
$\dot{r}$ = instantaneous linear burning rate of propellant
$\dot{r}_0$ = steady-state linear burning rate of propellant
R_1 = $[\partial F_n/\partial\theta]_0$
R_2 = $[\partial^2 F_n/\partial\theta^2]_0$
R_3 = $[\partial^3 F_n/\partial\theta^3]_0$
$Re(\mu/\epsilon)$ = real part of acoustic response function
t = time
T = temperature
T_f = propellant flame temperature
T_s = temperature at the solid surface
T_∞ = initial temperature of the propellant
W_1 = defined by Eq. (37)
x = distance into the solid from the surface
X_1 = defined by Eq. (38)
Y_1 = defined by Eq. (A4)
Z_1 = defined by Eq. (A5)
α = propellant thermal diffusivity
α_d = $d \ln P_c/dt$ during the decay of the acoustic pressure oscillations
α_g = $d \ln P_c/dt$ during the growth of the acoustic pressure oscillations
Δ = perturbation parameter
ϵ = P/P_0
ϵ_1 = amplitude of the fundamental pressure oscillations
ϵ'_1 = instantaneous value of ϵ_1
ϵ_2 = amplitude of the first harmonic pressure oscillations
ϵ'_2 = instantaneous value of ϵ_2
ζ = $\dot{r}_0 x/\alpha$
θ = $(T - T_\infty)/T_{s^0} - T_\infty)$
θ'_1 = component of temperature oscillating with fundamental
θ_1 = amplitude of fundamental surface temperature oscillation
λ = $8\pi\alpha f/\dot{r}_0^2 = 4i\lambda(\lambda_1 - 1)$
λ_1 = $\lambda_1^r + i\lambda_1^i$
μ_1 = fundamental amplitude of μ

Received April 24, 1968; February 18, 1970. This work was supported by the U. S. Army Ballistic Research Laboratory under Contract DA-04-200-AMC 968(X).

* Chief, Combustion Research Section, Propulsion Research Branch. Member AIAA.
† Senior Staff Scientist, Physical Sciences Laboratory.

ρ = propellant density
τ = dimensionless time $\dot{r}_0^2 t/4\alpha$

Superscripts

1 = instantaneous value
* = complex conjugate
m = component which changes steady state
sc = component which oscillates with first harmonic
i = imaginary component
r = real component

Subscripts

0 = value at steady state
1 = value of first-order coefficient
2 = value of second-order coefficient
3 = value of third-order coefficient

Introduction

UNSTABLE combustion of solid rocket propellants is of interest for two reasons: 1) it is one of several methods available for investigating solid propellant combustion; and 2) unstable combustion has presented serious problems in the development of some operational solid propellant rocket motors. Certain aspects of this problem, namely pressure-coupled combustion instability have been studied with the principal objective to examine the relationship between combustion instability, as observed by pressure oscillations in the gas phase, and exothermic reactions occurring on and near the solid phase surface.

Experimental studies have been directed toward investigating the effects of coating the solid oxidizer crystals, the chemical and physical nature of the propellant binder, catalysts, and cross-linking agents on the acoustic admittance. Concurrent theoretical studies have been directed toward predicting the effects of these variables on the acoustic response function. Additional analytical studies were conducted to study the transition from linear to nonlinear acoustic response as the amplitude of the pressure oscillations increases.

Theoretical Studies

Several investigators have considered theoretically the response of the propellant combustion zone to an oscillating pressure.[1-8] As a result of these studies, several combustion models have been analyzed for their transient combustion behavior. The principal approach taken in these studies has been to assume that specific physical and chemical processes control the combustion. The equations describing these processes are then noted and solved to permit calculation of the transient burning rate behavior, i.e., the acoustic response functions in an oscillating pressure field. These calculations require that certain physical and chemical properties of the combustion process are available from separate theoretical or experimental studies. These parameters generally characterize the gas-phase combustion zone and the surface gasification process but differ in the various proposed models. Since they are not available from separate experiment more recent efforts[9,10] have been directed towards comparing available transient burning rate data with the various theoretical predictions, thereby deriving the combustion parameters from the data.

A more direct approach, which minimizes the specific assumptions concerning the detailed structure at the combustion zone, results from a mathematical formulation which contains a number of parameters which have only very general definitions in physical terms. They can be derived from the experimental data and, by examination of a number of possible physical definitions, some further insight into the combustion zone behavior can be obtained. The principal advantage of this approach is that one is not committed to a specific model; instead, the experimental evidence guides the theoretical development. Also, by limiting the number of physical assumptions, one can better test their validity.

General Combustion Analysis

A general approach was taken in this work in which the only assumptions made in the analysis are those which were absolutely necessary to formulate the mathematics of the problem. For the purposes of analysis, the solid phase within the combustion zone is assumed to be characterized by the transient one-dimensional heat conduction equation

$$\partial T/\partial t = \alpha(\partial^2 T/\partial x^2) + \dot{r}(\partial T/\partial x) \tag{1}$$

At the solid surface, the rate at which the energy is transferred into the solid is given by

$$-k(\partial T/\partial x)_{x=+0} = N(T_s,P,T_f) \tag{2}$$

The function N contains the effects of energy transfer from the gas-phase combustion processes as well as the energetics of any surface reaction/vaporization processes. Also, deep within the propellant the temperature is not influenced by the combustion process. Thus

$$T \to T_\infty \text{ as } x \to \infty \tag{3}$$

Within the gas phase, it is generally possible to characterize the burning rate at constant conversions‡ by the general expression

$$\dot{m}_g = J(T_s,P,T_f)\rho \tag{4}$$

The specific details of the gas-phase combustion will determine the particular functional form, but most gas-phase combustion models, be they diffusion or premixed flames, will follow this general relationship.

At the solid surface, the rate of gasification can be expressed by

$$\dot{r} = H(T_s,P) = \dot{m}_s/\rho \tag{5}$$

Equations (1–5) constitute a general combustion model in which the only assumptions concerning the chemistry and physics of the process are that the bulk solid is homogeneous and nonreactive. These equations can now be solved for the transient burning rate and gas temperature response to a pressure disturbance. First, since $\dot{m}_g = \dot{m}_s$, Eqs. (4) and (5) can be combined to yield an expression for the gas temperature in terms of the pressure and surface temperature

$$T_f = G(T_s,P) \tag{6}$$

Substituting Eq. (6) into Eq. (2) yields

$$-k(\partial T/\partial x)_{x=+0} = F(T_s,P) \tag{7}$$

The analysis can be simplified further by normalizing the characterizing equations to yield

$$\partial\theta/4\partial\tau = (\partial^2\theta/\partial\zeta^2) + H_n(\theta_s,\epsilon)(\partial\theta/\partial\zeta) \tag{8}$$

$$H_n(\theta_s,\epsilon) = \dot{r}/\dot{r}_0 \tag{9}$$

$$-(\partial\theta/\partial\zeta)_{\zeta=+0} = F/F_0 = F_n(\theta_s,\epsilon) \tag{10}$$

It should be noted that Hart and co-workers[8] have used a similar approach for characterizing the gas phase portion of the combustion zone. In addition they used an Arrhenius relation to characterize the complex surface gasification process. However, this is an unnecessary restriction on their analysis, as the following development will show.

‡ The usual assumption has been that the conversion of "reactants" to "products" (i.e., the extent to which the gasified "reactants" are converted to "products" in the gas phase reaction zone) is constant, even under transient conditions. This may not be a valid assumption.

To solve Eqs. (8–10) the dependent variables can be expanded in a Taylor series, i.e.,

$$\theta = 1 + \Delta\theta_1 + \Delta^2\theta_2 + \Delta^3\theta_3 + \ldots \quad (11)$$

In a similar manner, the functions H_n, F_n, and G_n can be expanded by a Taylor series to yield a series of simultaneous equations characterizing the burning rate behavior.

Linear Response

The linear response of this set of equations can be determined by collecting terms of the order Δ, i.e.,

$$\frac{1}{4}\frac{\partial\theta_1}{\partial\tau} = \frac{\partial^2\theta_1}{\partial\zeta^2} + \frac{\partial\theta_1}{\partial\zeta} + [\theta_1^0 A_1 + \epsilon_1' Q_1]\frac{d\theta_0}{d\zeta} \quad (12)$$

$$-(\partial\theta_1/\partial\zeta)_{\zeta=+0} = \theta_1^0 R_1 + \epsilon_1' B_1 \quad (13)$$

Assuming that the pressure oscillates as

$$\epsilon_1' = \epsilon_1 \exp(i\lambda\tau) \quad (14)$$

one obtains the equation for the linear response (i.e., the acoustic response function)

$$\mu_1/\epsilon_1 = [A_1B_1 + Q_1(\lambda_1 - R_1)]/[\lambda_1 + A_1\lambda_1^{-1} - R_1] \quad (15)$$

The corresponding equations for the burning rate pressure exponent, surface temperature and flame temperature amplitudes are

$$n[1 + A_1 - R_1] = A_1B_1 + Q_1(1 - R_1) \quad (16)$$

$$(\theta_1/\epsilon_1) = [(\mu_1/\epsilon_1) - Q_1]/A_1 \quad (17)$$

$$\left[\frac{T_f - T_f^0}{T_f^0\epsilon_1}\right] = \left[\frac{T_f - T_f^0}{T_f^0\epsilon_1}\right]_{\lambda=0} + \left[\left(\frac{\mu_1}{\epsilon_1}\right) - n\right]\left[\left(\frac{\partial G}{\partial\theta}\right)_0 \Big/ A_1\right] \quad (18)$$

It should be noted that a detailed knowledge of the structure of the gas phase combustion zone or the surface degradation process is not required to characterize the acoustic response function and the entropy wave behavior of the combustion process. These general definitions of the combustion parameters explain why Culick[11] was able to show that most proposed combustion models could be placed in the form of Eq. (15). If $Q_1 = 0$, the result reduces to the form discussed in several recent reports and papers, with a slight redefinition of the parameter B_1.

The solution to Eqs. (12–14) also shows that the two criteria for the region of intrinsic stability are

$$4A_1 > R_1^2 \quad (19)$$

$$2A_1 > R_1(R_1 - 1) \quad (20)$$

If these conditions are not satisfied, any perturbation in the combustion process, regardless of the source, will cause runaway burning rates. They form a boundary for realistic values of A_1 and R_1 which can be ascribed to real propellants.

Second-Order Behavior

Collecting terms of the order Δ^2 yields

$$\frac{1}{4}\frac{\partial\theta_2}{\partial\tau} = \frac{\partial^2\theta_2}{\partial\zeta^2} + \frac{\partial\theta_2}{\partial\zeta} + \mu_1\frac{\partial\theta_1}{\partial\zeta} + \frac{\mu_2}{2}\frac{d\theta_0}{d\zeta} \quad (21)$$

$$-\left(\frac{\partial\theta_2}{\partial\zeta}\right)_{\zeta=+0} = \frac{(\theta_1^0)^2}{2}R_2 + \epsilon'_1\theta_1^0 D_{11} + \frac{\epsilon'^2_1}{2}B_2 + \theta_2^0 R_1 + \epsilon_2' B_1 \quad (22)$$

These equations are linear in the unknown θ_2, but nonlinearities appear in the form of the cross products of first-order terms. In the solution of the first-order problem, the dimensionless temperature was given by $\theta_1^0 = \theta_1 \exp(i\lambda\tau)$. However, Eqs. (21) and (22) were derived using the real part of θ_1^0. Hence, as Friedly[12] has shown, the cross products of the first-order terms must be considered as

$$[Re(\theta_1^0)]^2 = \frac{Re(\theta_1\theta_1^*)}{2} + Re\,\frac{(\theta_1)^2}{2}\exp(2i\lambda\tau) \quad (23)$$

Equation (23) shows that the solution of the second-order problem can be divided into two parts and solved separately. One part reflects the change in the time average burning rate and the other reflects the component which oscillates with the first harmonic frequency.

After making the appropriate substitutions into Eqs. (21) and (22), the change in the time average surface temperature and hence the time average burning rate can be determined.

$$\dot{r}/\dot{r}_0 = 1 + E(\lambda)\epsilon_1^2 \quad (24)$$

The detailed expression for $E(\lambda)$ is presented in Appendix A. It contains six combustion constants, in addition to those which characterize the linear response, which result from the second-order expansions of Eqs. (5) and (7).

Third-Order Behavior

Following a similar procedure, the terms of order Δ^3 can be collected. The result consists of two terms, one which oscillates with the fundamental and one which oscillates with the second harmonic. The first term, the one oscillating at the fundamental, is of particular interest because it represents the change in the fundamental response with pressure amplitude. Thus

$$Re(\mu_1/\epsilon_1) = [Re(\mu_1/\epsilon_1)]_{\lim\epsilon_1\to 0} + \epsilon_1^2 F(\lambda) \quad (25)$$

where $F(\lambda)$ represents the component of μ_3 oscillating with $\exp(i\lambda\tau)$. The detailed equation for $F(\lambda)$ is also presented in Appendix A. This expression contains eight constants from the third-order expressions of Eqs. (5) and (7) as well as the constants from the first- and second-order expansions.

The result of this mathematical development is a very general framework for the study of combustion instability phenomena. No assumption concerning the physics and chemistry of the gas phase and surface energy effects was made, nor was the nature of the surface gasification specified. The principal assumptions are that the solid is homogeneous and nonreacting and that the time constants for the gas phase processes are sufficiently fast so that the gas phase is always in equilibrium with the instantaneous pressure and solid surface conditions.

Experimental Studies

Since the mathematical framework contains constants which are not defined physically, they must be determined by a comparison with experimental data. Furthermore, a study of the influence of propellant formulation changes on these constants should provide insight into the physical processes controlling combustion. This was the approach taken in this part of the study.

There are several potential methods for altering the contributions of various chemical reactions to the acoustical response. One method involves coating the oxidizer crystals to alter the reactivity of the crystal-binder interface. Also, changes in the chemical structure of the binder, in the agents used to crosslink the binder, in catalyst type and content, and in ammonium perchlorate particle size and loading were all postulated to influence the acoustic response function. Accordingly, propellants were prepared which permitted investigation of these variables. Table 1 describes the propellants tested in these studies.

Comparison of Theory and Experiment

The experimental apparatus and the data reduction procedure were described previously.[5,13] A comparison of the

Table 1 Propellant formulations

Propellant no.	Composition binder oxidizer	Oxidizer particle size	Oxidizer coating		Propellant additive	$\dot{r}$ at 200 psi in./sec	n at 200 psi	Binder/ curative
			Polymer, %	Additive, %				
1	22/78	190	0	0	0	0.113	0.49	CTPB/MAPO
2	22/78	190	1.5 Kel-F	0	0	0.116	0.55	CTPB/MAPO
3	22/78	100	0	0	0	0.129	0.58	CTPB/MAPO
4	22/78	190	1 Kel-F	1 Cab-O-Sil	0	0.170	0.61	CTPB/MAPO
5	22/78	190	1 Kel-F	2 LiF	0	0.063	0.78	CTPB/MAPO
6	22/78	190	1.5 Hypalon	0	0	0.128	0.52	CTPB/MAPO
7	22/78	190	1.5 Ethyl Cellulose	0	0	0.137	0.51	CTPB/MAPO
8	22/76.5	190	0	0	0.77% Kel-F 0.77% Cab-O-Sil	0.158	0.63	CTPB/MAPO
9	22/76.8	190	0	0	1.2% Kel-F	0.110	0.42	CTPB/MAPO
10	22/78	190	3.0 Kel-F	0	0	0.120	0.51	CTPB/MAPO
11	22/78	190	1.5 Viton A	0	0	0.108	0.45	CTPB/MAPO
12	22/78	190	0	0	0	0.145	0.50	PBAN/Epoxy
13	22/78	190	0	0	0	0.127	0.50	PBAN/MAPO
14	22/78	190	0	0	0	0.138	0.42	CTPB/Epoxy
15	16/84	70% 190 30% 8	0	0	0	0.126	0.30	UTREZ/Cure 1
16	16/84	65% 190 35% 8	0	0	0	0.130	0.37	UTREZ/Cure 2
17	16/84	65% 190 35% 8	0	0	0	0.24	0.21	PEP
18	16/84	65% 190 35% 8	0	0	0.25% Fe_2O_3	0.156	0.36	UTREZ/Cure 2
19	16/84	65% 190 35% 8	0	0	0.50% Fe_2O_3	0.188	0.38	UTREZ/Cure 2
20	16/84	65% 190 35% 8	0	0	0.25% Copper Chromite	0.179	0.49	UTREZ/Cure 2
21	16/84	65% 190 35% 8	0	0	0.50% Copper Chromite	0.182	0.51	UTREZ/Cure 2
22	16/84	65% 190 35% 8	0	0	0.13% Copper Chromite	0.173	0.47	UTREZ/Cure 2
23	16/84	65% 400 35% 8	0	0	0	0.10	0.18	UTREZ/Cure 2

experimental results from the T-burner was made with Eqs. (15) and (16). A parametric study of these equations shows that the maximum value of the acoustic response function depends on both Q_1 and R_1 and that the frequency at which this maximum occurs depends on A_1 and Q_1. In these calculations, n was held constant and B_1 was determined from Eq. (16) for the particular set of A_1, R_1, Q_1. Since there is no simple method for deriving the set of combustion parameters graphically, the best set of A_1, R_1, Q_1 was selected by the least-squares approach based on a comparison of the measured and predicted real parts of the response function. The best set of combustion parameters derived for each propellant is shown in Tables 2 and 3. All the data were obtained using a value of the thermal diffusivity of 3.0×10^{-4} in.^{2}/sec.

Because Eqs. (15) and (16) are nonlinear in the combustion parameters, the process of selecting the minimum value of the error estimate (i.e., the sum of squares) is not straightforward. Of the several methods for minimizing a nonlinear function, the grid approach was selected as being the simplest and most straightforward. The region of A_1, R_1, Q_1 most likely to contain the minimum was mapped, and the set of A_1, R_1, Q_1 yielding the minimum error estimate was determined. This result represents a "local" minimum which may not be the "universal" minimum which represents a different "best" set. This is illustrated by the fact that two solutions were obtained for propellant 7. In this case, the solution $A_1 = 18$, $R_1 = 2.0$, $Q_1 = 3.6$ yielded the lower error estimate.

Propellant 5 illustrates another problem which can be encountered. Only four measurements were obtained for this propellant: two each at two different frequencies. Unfortunately, there was not a significant difference in the measured response functions at the two frequencies. Thus, one could draw the response function-frequency curve with the maximum between the two sets of points, or one could consider that there is a large error between the sets and draw the curve most anywhere. Therefore, no best solution could be found for this propellant.

In an effort to insure that the "universal best" set of combustion parameters was determined, a wide range of values was examined. However, there is always the possibility that the grid was too large and that points of low error estimates were overlooked. It should also be noted that propellants for which the maximum response function was clearly determined did not present any problem, but those without a clearly established maximum (i.e., propellants 5 and 7) did present difficulties.

All of the values presented in Tables 2 and 3 satisfy the stability criteria defined by Eqs. (19) and (20) and, thus, represent values which are in the region of inherent stability.

Statistical Significance of Q_1

Many of the values of Q_1 in Tables 2 and 3 are negative, which is difficult to explain on physical grounds. However, it is possible that the values of Q_1 presented in Tables 2 and 3 are not significantly different than zero.

To test the hypothesis, the data were examined by the grid approach for the case of $Q_1 = 0$. The values of A_1, R_1, and B_1 obtained for this special case are shown in Tables 4 and 5. The error estimates for the general case and for the case where Q_1 is zero were compared statistically using the "F" test. At the 95% confidence level, propellants 8, 14, 15, 16, 17, 19, 21, 22, and 23 (i.e., those marked with a flag in Tables 2 and 3) have values of Q, significantly different than zero. In all the other cases, one cannot distinguish the derived values of Q_1 from zero.

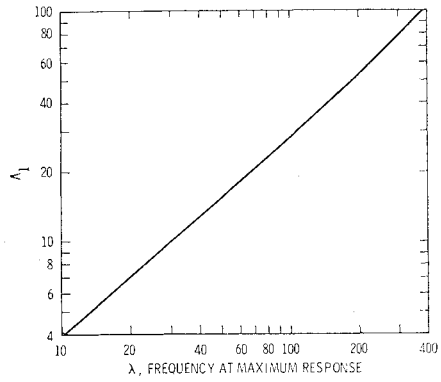

Fig. 1 Frequency of maximum acoustic response vs A_1.

Comparison of Data Reduction Method with Other Approaches

Several alternate data reduction approaches to the one used in this program have been proposed by other investigators. With the exception of the limited efforts of Hart and co-workers,[8] these comparisons have all been made assuming $Q_1 = 0$. As shown in the preceding section, this is valid in some, but not all, cases.

If $Q_1 = 0$, then one approach to the comparison of Eq. 15 with experimental data involves determining both the real and the imaginary parts of the response function from experimental data. For the T-burner, Strittmater,[14] Friedly,[15] and Beckstead[9] have shown that

$$\frac{\mu}{\epsilon} \approx \frac{P}{4\rho c \dot{r}_0}\left[\frac{\alpha_g + \alpha_d}{f_d} + 2\pi i \frac{(f_g - f_d)}{f_d}\right] \tag{26}$$

Since the growth and decay constants (i.e., α_g and α_d) and the corresponding frequencies are determined experimentally for each point, equating the real and imaginary parts of Eqs. (15) and (26) provides the two expressions in terms of R_1 and A_1 from which both combustion parameters can be derived.

This approach to the analysis of T-burner data has a serious limitation resulting from experimental uncertainties. For the propellants, shown in Table 1, the imaginary part of Eq. (26) becomes

$$Im(\mu/\epsilon) \approx 400\ (f_g - f_d)/f_d \tag{27}$$

Since f_g and f_d have similar magnitudes, the experimental errors in both f_g and f_d are magnified in the calculation of $Im(\mu/\epsilon)$. This results in significant uncertainties in R_1 and A_1. Thus, it was concluded that this method of data reduction, though more rigorous, is too sensitive to small errors in the frequency measurements. For this reason, the analysis

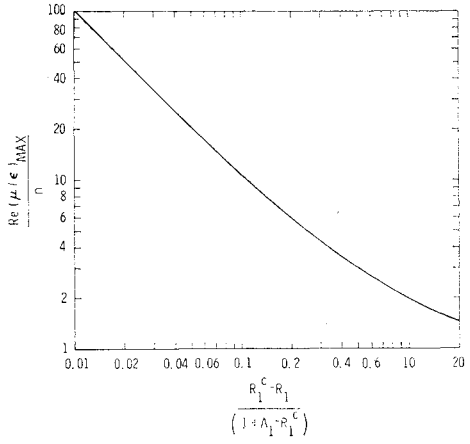

Fig. 2 Maximum value of acoustic response function.

Table 2 Linear combustion parameters at 200 psig

Propellant no.	$A_1 \pm 2$	$R_1 \pm 0.2$	$Q_1 \pm 0.2$	B_1
1	60	7.0	−0.3	0.41
2	32	4.4	−0.3	0.46
3	24	5.2	0.2	0.48
4	26	5.0	−0.4	0.45
5		No unique solution		
6	14	4.4	1.0	0.62
7	30	4.6	1.6	
	18	2.0	3.6	0.57
8	12	3.2	2.4[a]	0.95
9	36	6.2	1.3	0.55
10	34	3.6	−0.5	0.43
11	28	5.2	−0.1	0.37
12	24	1.8	−0.3	0.47
13	14	3.0	1.0	0.57
14	18	5.8	0.6[a]	0.47
15	38	7.6	0.6[a]	0.35
16	36	6.7	−0.5[a]	0.23
17	8	3.4	1.0[a]	0.45
18	22	5.4	0.1	0.31
19	10	4.2	0.1[a]	0.29
20	18	−0.4	0.0	0.53
21	12	4.6	0.3[a]	0.45
22	28	0.4	−0.7[a]	0.50
23	20	6.2	1.3[a]	0.47

[a] Significant at 95% confidence level.

of the imaginary part of the response function was not included in the data reduction procedure.

In an effort to circumvent this difficulty, Beckstead and Culick[9] have modified this approach. Instead of using the imaginary part of the response function they noted that $Im(\mu/\epsilon) \approx 0$. The present data were also reduced using both Eqs. (26) and (27) and the influence of small errors in the frequencies on $Im(\mu/\epsilon)$ was determined. For frequencies below 800–1000 cps these resulting errors in $Im(\mu/\epsilon)$ have little effect on A_1, but some significant changes in R_1 were noted. At higher frequencies changes in both A_1 and R_1 were observed. In some cases these small frequency changes caused the values to shift across the boundary between intrinsic instability and intrinsic stability. It is interesting to note that Beckstead and Culick[9] derived combustion parameters in both regions in the analysis of their data, clearly a physically unacceptable situation. This error analysis, however, indicates that the probable source of the difficulty is the data reduction procedure and in particular the effects of errors in $Im(\mu/\epsilon)$. On this basis use of Eq. (27) in the analysis of the data has been rejected until more accurate measurements are available.

In another study, Oberg[16] has compared experimental data reduced using only the real part of Eq. (26) with Eq. (15) ($Q_1 = 0$). He concluded that both the T-burner data obtained by Horton[17] and the L^* data obtained by Beckstead[18] can be adequately correlated by Eq. (15).

Approximate Method for Data Reduction

In the course of studying various data reduction methods, a quick and accurate method was developed in which $Q_1 = 0$ is assumed. Under these conditions, parametric solutions of Eq. (15) show that, to a good approximation, the response is

Table 3 Effect of pressure on combustion parameters (propellant 1)[a]

Pressure, psia	$A_1 \pm 0.2$	$R_1 \pm 0.2$	$Q_1 = \pm 0.2$	B_1
100	40	7.8	−0.7	0.27
200	60	7.0	−0.3	0.41
500	20	5.2	0.0	0.39

[a] Significant at 95% confidence level.

Table 4 Linear combustion parameters at 200 psig ($Q_1 = 0$)

Propellant no.	$A_1 \pm 2$	$R_1 \pm 0.2$	B_1
1	56	6.6	0.44
2	28	4.2	0.49
3	24	5.4	0.43
4	24	4.6	0.52
5	No unique solution		
6	20	5.2	0.41
7	40	6.8	0.44
8	20	5.6	0.48
9	52	8.4	0.36
10	30	3.0	0.48
11	26	5.4	0.37
12	20	1.6	0.49
13	28	3.2	0.46
14	24	6.0	0.33
15	40	8.2	0.25
16	32	5.6	0.32
17	26	6.2	0.17
18	22	5.6	0.29
19	12	4.0	0.29
20	18	−0.4	0.53
21	14	4.6	0.38
22	16	1.6	0.42
23	36	7.8	0.15

a maximum when $Im(\mu_1/\epsilon_1) = 0$. Hence,

$$A_1 = \lambda\lambda_1{}^i/4(\lambda_1{}^r - 1) \tag{28}$$

where λ_1 is evaluated at the frequency of maximum response. A plot of Eq. (28) is shown in Fig. 1. Therefore, the parameter A_1 can be determined directly from experimental data by noting the dimensionless frequency at which $Re(\mu/\epsilon)$ becomes a maximum. The parameter R_1 can then be determined from the maximum response function and burning rate pressure exponent by substituting Eq. (28) into Eqs. (15) and (16), yielding

$$(1/n)\, Re(\mu/e)_{\max} = (1 - R_1 + A_1)/\{\lambda_1{}^r - R_1 + 4A_1\lambda_1{}^i/\lambda\} \tag{29}$$

Equation (29) is shown graphically in Fig. 2 where $R_1{}^c$ is the positive value of R_1 derived from Eq. (20).

The values derived by this method are nearly identical to those presented in Tables 4 and 5 ($Q_1 = 0$) which were derived by the least-squares approach.

Analysis of Error Effects

For reasons of simplicity and economy, the approximate method presented in the preceding section was used in this part of the study. The effect of errors in the dimensionless frequency at the maximum response (i.e., burning rate, diffusivity, and dimensional frequency errors) were determined by an arbitrary 16% reduction in α and, therefore, the dimensionless frequency at the maximum response. The results show that an error of 16% in λ results in a 16% error in A_1 and an 8% error in R_1.

The response function-frequency curve was calculated for propellant 1 using the derived combustion parameters shown in Table 4. Figure 3 shows that the shape of the predicted response frequency curve is not significantly altered by an

Table 5 Effect of pressure on combustion parameters (propellant 1 with $Q_1 = 0$)

Pressure, psig	$A_1 \pm 2$	$R_1 \pm 0.2$	B_1
100	44	7.8	0.42
200	56	6.6	0.44
500	20	5.2	0.39

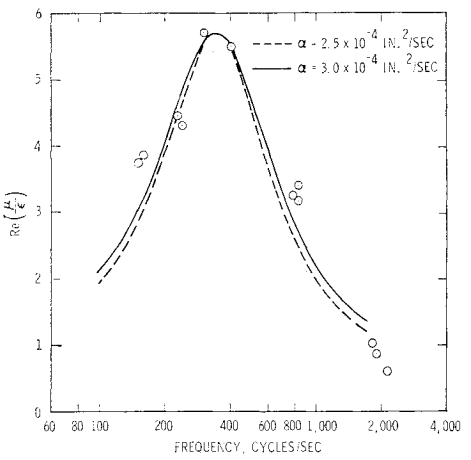

Fig. 3 Effect of thermal diffusivity on shape of response-frequency curve.

error in α. Figure 4 shows the effect of n and $Re(\mu/\epsilon)_{\max}$ on the predicted response function frequency curve. The pressure exponent, n, influences the shape of the curve at the frequency extremes but has little influence near the maximum; $Re(\mu/\epsilon)_{\max}$ has more influence on the peak region of the curve but little influence on the frequency extremes.

Figures 3 and 4 show that the response function derived from Eqs. (15) and (16) adequately predicts the observed shape of the frequency-response function curve. Other comparisons between the data on the curves predicted by Eqs. (15) and (16) using the combustion parameters shown in Table 2 are in agreement. This leads to the conclusion that Eqs. (15) and (16) adequately represent the linear combustion behavior of the propellants listed in Table 1, assuming $Q_1 = 0$.

Interpretation of Combustion Parameters

It is important to interpret the physical significance of the various linear combustion parameters and the numerical values of the associated physical parameters. The parameters associated with the burning rate of the solid phase, (i.e., A_1 and Q_1), can be considered. If one assumes that

$$\dot{r}_s = H(T_s,P) = Z_2P_1{}^{n1} \exp(-E_2/RT_s) \tag{30}$$

then

$$A_1 = E_2(T_{s0} - T_\infty)/RT_{s0}{}^2 \tag{31}$$

$$Q_1 = n^1 \tag{32}$$

The parameter A_1 is a measure of the surface temperature and activation energy of the reaction. Assuming an initial propellant temperature of 300°K and a steady-state surface temperature of 750°K, a value of A_1 equal to 30 corresponds

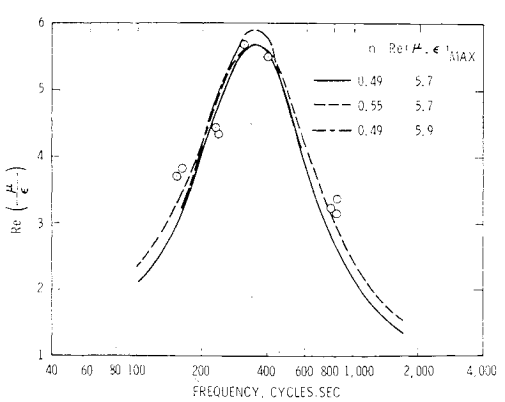

Fig. 4 Effect of steady-state burning rate exponent and $Re(\mu/\epsilon)_{\max}$ on shape of response-frequency curve.

to an E_2 of 74.5 kcal/mole. If the surface temperature is assumed to be 850°K, then an A_1 of 30 corresponds to an E_2 of 78.1 kcal/mole. Thus, in the case of Eq. (30), the variations in A_1 shown in Table 2 and 3 reflect formulation effects on E_2 and not effects on the surface temperature. At a 750°K surface temperature, the activation energies derived from Table 1 range from 20 kcal/mole for propellant 17 to 145 kcal/mole for propellant 1. These are extremely high, especially in view of the values reported for the decomposition and gasification of various ingredients. The results, though consistent with nonacoustic combustion instability data,[9] suggest that there is a complex series of surface reactions and that the formulation changes and pressure shift the balance rather drastically.

Further evidence of this shift in the reaction process is provided by the catalyst data in Table 2. These data show that the addition of catalysts to the formulation decreases the value of A_1; the higher the catalyst concentration the lower the value of A_1. At the same time, Q_1 is increased from -0.5 to approximately 0.1 when the catalysts are present in concentrations greater than 0.25%. Since the parameters A_1 and Q_1 reflect the solid phase contribution to the mass burning rate, the effects of burning rate catalysts influence this part of the combustion process in addition to the gas phase reaction effects.

Also, the effect of pressure on A_1, as shown in Table 3, suggests the complexity of the surface reaction process. The large changes in A_1 indicate that the mechanism of the surface gasification process shifts drastically with pressure. Furthermore, the change does not appear to be monotonic with pressure.

The data in Table 2 indicate that the effect of pressure (i.e., Q_1) is significant at the higher solids loading. At 78% oxidizer loading, only two of the propellants showed Q_1 values significantly different than zero. At 84%, however, seven of the nine propellants had Q_1 values significantly different than zero. This suggests that the oxidizer loading determines the pressure dependence of the surface gasification process.

A perplexing aspect of these data is the fact that some of the significant nonzero values of Q_1 are negative, while some are greater than one in other cases. The latter result may be somewhat surprising, but it can be explained in terms of possible chemical reaction mechanisms. The explanation of the former result (i.e., that $Q_1 < 0$) is not possible in this manner. This difficulty in explaining the activation energy and the order of the reaction leads one to question the validity of Eq. (30) in characterizing propellant combustion. However, logical alternates to Eq. (30) are equally difficult to propose.

The situation regarding R_1 and B_1 is even more complex. To demonstrate this point, consider the first-order Taylor expression of Eq. (2)

$$dN = \left(\frac{\partial N}{\partial T_s}\right)_0 dT_s + \left(\frac{\partial N}{\partial P}\right)_0 dP + \left(\frac{\partial N}{\partial T_f}\right)_0 dT_f \quad (33)$$

Equation (33) can then be combined with the first-order expansions of Eqs. (2) and (4) to provide alternate definitions of R_1 and B_1 in terms of the functions $N(T_s,P,T_f)$, $H(T_s,P)$, and $J(T_s,P,T_f)$.

$$R_1 = \frac{\left(\frac{\partial N}{\partial T_s}\right)_0\left(\frac{\partial J}{\partial T_f}\right)_0 + \left(\frac{\partial N}{\partial T_f}\right)_0\left[\left(\frac{\partial H}{\partial T_s}\right)_0 - \left(\frac{\partial J}{\partial T_s}\right)_0\right]}{\dot{r}_0\rho c_p(\partial J/\partial T_f)_0} \quad (34)$$

$$B_1 = \left\{\frac{\left(\frac{\partial N}{\partial P}\right)_0\left(\frac{\partial J}{\partial T_f}\right)_0 + \left(\frac{\partial N}{\partial T_f}\right)_0\left[\left(\frac{\partial H}{\partial P}\right)_0 - \left(\frac{\partial J}{\partial P}\right)_0\right]}{\dot{r}_0\rho c_p(T_s - T_\infty)(\partial J/\partial T_f)_0}\right\}P_0 \quad (35)$$

Considering the wide range of proposed definitions for the parameters in Eq. (33) one finds that generally $(\partial H/\partial T_s) > (\partial J/\partial T_s)$, that $(\partial N/\partial T_f) > 0$, and that $(\partial J/\partial T_f) > 0$. Hence, one can conclude that if $R_1 < 0$, then $(\partial N/\partial T_s) < 0$. This would be the case, for example, if Eq. (30) applies and the process is endothermic. However, since the experimental value of $R_1 > 0$, this implies that approximately $(\partial N/\partial T_s) \geq 0$. This then suggests that the surface processes are at least nearly thermally neutral or perhaps even somewhat exothermic. The magnitude of the various partial derivatives determine the extent to which this is true. However, it would appear that the values of R_1 are reasonable in terms of the various proposed definitions from the several available combustion models. Similarly, the values of B_1 derived from the data are also quite reasonable. Both the granular diffusion or the laminar premixed flame models predict pressure indices between 0 and 1, which is consistent with the observations.

Examination of the effects of the various formulation changes on R_1 and B_1 yields some interesting results. The effect of coatings on the solid oxidizer can be considered first. The coatings reduced the temperature sensitivity of the heat transfer into the solid phase. Viton A was the least effective, and Kel-F, Hypalon, and ethyl cellulose all had nearly the same effect. It is, of course, impossible to determine whether the effect is the result of a reduction in possible exothermic surface reactions (the original intent of the experiment) or the result of decreased mixing within the gas phase reaction zone. There appears to be little effect of the coatings on B_1, so no clues can be obtained from studying those results. It should be noted that the coatings were porous, thereby lessening the resulting effects in comparison to a nonporous coating.

The influence of the catalysts is also interesting to consider. In all cases, the values of R_1 were substantially reduced by the addition of the catalysts. When combined with the catalyst influence on the activation energy of the surface gasification process, the data suggest the effect is to reduce the activation energies of the various reactions. An additional influence, which affects R_1 but not A_1, results from increasing the gas phase damping. Both catalysts exist as solids within the gas phase combustion zone and might behave in much the same manner as aluminum.

The addition of copper chromite yields substantially lower values of R_1 and higher values of B_1 than the corresponding iron catalized propellants. It may be that copper chromite influences different processes characterized in R_1 and B_1 than iron oxide.

The influence of pressure on R_1 and B_1, at least for propellants 1, seems to be counter to expectations. Increasing the pressure appears to decrease R_1 in the region where one would expect the self-deflagration of AP to increase R_1. (However, the shift in the complex reaction path and the resulting change in activation energies could cause the effect to be opposite to the anticipated effect.)

Interpretation of Nonlinear Behavior

Eisel[19] has found experimentally that $-0.5 < E(\lambda) < 0$ for both composite and double-base propellants. Therefore, parametric studies were conducted to define a reasonable range of the second-order combustion parameters, i.e., R_2, B_2, and D_{11} in Eq. (22) and the corresponding second-order coefficients from the expansion of Eq. (5). In Appendix A it is shown that the six second-order constants could be combined to two independent parameters by assuming that $\epsilon_2 = 0$ and by noting that, if $\dot{r}_0 = aP_0^n$ one obtains

$$E(0) = n(n-1)/4 \quad (36)$$

These parameters are

$$W_1 = (1 - R_1)A_2 + A_1R_2 \quad (37)$$

$$X_1 = (1 - R_1)C_{11} + A_1D_{11} \quad (38)$$

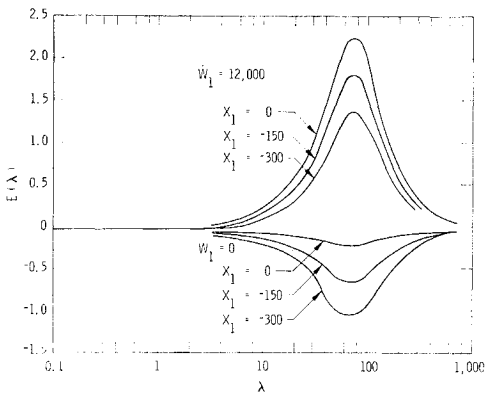

Fig. 5 Nonlinear effect on steady-state burning rate.

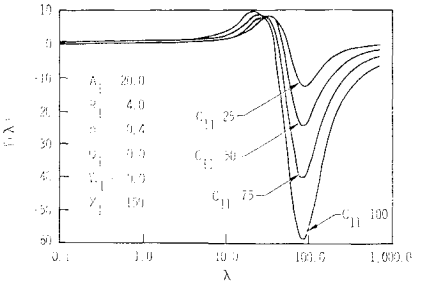

Fig. 6 Nonlinear effect on acoustic response function.

The effects of W_1 and X_1 on $E(\lambda)$ are shown in Fig. 5 assuming $A_1 = 20$, $R_1 = 4.0$, $Q_1 = 0$, and $n = 0.4$.

These results show that both increases and decreases in the time average burning rate can be explained within this analytical framework depending on the nonlinear constants. It should be noted that in all cases the limit of $E(\lambda)$ as the frequency approaches zero corresponds to the shift consistent with the Eq. (36). Only limited experimental data are available with which to compare these predicted results. When compared with Fig. 5 and other parametric results not shown, Eisel's data indicate that W_1 is less than 200 for these propellants.

In addition to the second-order effects, the third-order behavior has been examined to study the behavior of $F(\lambda)$ for various combustion parameters. The expansion of Eqs. (5) and (7) yields eight constants in addition to the first- and second-order constants. A wide range of values was examined, but because of the large number of constants only a descriptive summary of the results will be presented.

In general, it was determined that $-50 < F(\lambda) < 50$ for reasonable values of the various combustion parameters. An example of the behavior of $F(\lambda)$ is shown in Fig. 6. Thus, theoretically at least, the acoustic response function can either increase or decrease with the increasing acoustic pressure found in the T-burner. For $F(\lambda) < 0$, the combustion process itself could limit the acoustic pressure amplitude. However, acoustic losses could also be responsible for the limiting amplitude. Current analyses and data do not permit these effects to be separated so experimental values for $F(\lambda)$ cannot be determined.

Conclusions

Transient combustion of composite solid propellants can be characterized by assuming the transient behavior of the solid phase to be that of a homogeneous nonreacting solid.

The gasification of the solid phase was found to be an extremely complex process. For all propellants tested, this process was found to be strongly dependent upon surface temperatures, more so than could be accounted for by an Arrhenius expression with a reasonable activation energy. For propellants having an 84% loading of AP, the gasification process was also dependent on pressure and surface temperature. Some propellants showed the gasification increasing with pressure, while others showed a decrease.

The rate of energy transfer into the solid was found to increase with increasing surface temperature and increasing pressure. The temperature effect is characteristic of a thermally neutral or slightly exothermic surface. The pressure effect is consistent with that predicted by laminar premixed and granular diffusion flame models. Coating the solid oxidizer reduced the temperature sensitivity of the energy transfer, with the magnitude of the effect depending on the coating. However, coatings had little effect on the pressure sensitivity.

Parametric studies were conducted in which the linear behavior was held constant and the effects of the second- and third-order coefficients were determined. The results show that both positive and negative values of $E(\lambda)$ can be obtained, depending on the magnitude of the constants. Since Eisel has observed $E(\lambda)$ to be negative in his studies, this defines the region of reasonable second-order coefficients. Additional studies show that $F(\lambda)$ was negative for reasonable second- and third-order coefficients.

Appendix A: Equations for Nonlinear Behavior

The second-order behavior of the general analysis [Eqs. (1–5)] is given by

$$E(\lambda) = Re\left\{\frac{1}{4(1 + A_1 - R_1)}\left[\left(\frac{\theta_1}{\epsilon_1}\right)\left(\frac{\theta_1}{\epsilon_1}\right)^* W_1 + 2\left(\frac{\theta_1}{\epsilon_1}\right) X_1 + Y_1 + 4\left(\frac{\epsilon_2^m}{\epsilon_1^2}\right) Z_1 - 2\left(\frac{\mu_1}{\epsilon_1}\right)^*\left(\frac{\theta_1}{\epsilon_1}\right) A_1\right]\right\} \quad \text{(A1)}$$

where

$$W_1 = (1 - R_1)A_2 + A_1R_2 \quad \text{(A2)}$$

$$X_1 = (1 - R_1)C_{11} + A_1D_{11} \quad \text{(A3)}$$

$$Y_1 = (1 - R_1)Q_2 + A_1B_2 \quad \text{(A4)}$$

$$Z_1 = [(1 - R_1)Q_1 + A_1B_1] \quad \text{(A5)}$$

However, by extrapolating $E(\lambda)$ to $E(0)$ one of the constants can be eliminated. Assuming $\epsilon_2^m = 0$ as $\lambda \to 0$, Z_1 is no longer important and the resulting expression becomes

$$E(0) = \frac{n(n-1)}{4} = \frac{1}{4(1 + A_1 - R_1)}\left\{\left(\frac{n - Q_1}{A_1}\right)^2 W_1 + 2\left(\frac{n - Q_1}{A_1}\right) X_1 + Y_1 - 2n\,\frac{n - Q_1}{A_1} A_1\right\} \quad \text{(A6)}$$

The corresponding solution for μ_2^{sc}/ϵ_1^2, the component of μ_2 which oscillates at the first harmonic, is

$$\frac{\mu_2^{sc}}{\epsilon_1^2}(\lambda_2 + A_1/\lambda_2 - R_1) = \left\{\frac{(\theta_1/\epsilon_1)^2[W_1 + A_2(\lambda_2 - 1)] + 2(\theta_1/\epsilon_1)[X_1 + C_{11}(\lambda_2 - 1)] + Y_1 + Q_2(\lambda_2 - 1)}{4}\right\} + \frac{\epsilon_2^{sc}}{\epsilon_1^2}\{n(1 + A_1 - R_1) + Q_1(\lambda_2 - 1)\} + \frac{(\mu_1/\epsilon_1)(\theta_1/\epsilon_1)}{2\lambda_1(\lambda_1 - 1)^2} A_1\left\{\frac{Dm(\lambda) - \lambda_2(\lambda_2 - \lambda_1)}{\lambda_2}\right\} \quad \text{(A7)}$$

where

$$D \equiv (\mu_1/\epsilon_1)/(\theta_1/\epsilon_1),\ m(\lambda) \equiv (\lambda_1 - 1)(\lambda_2 + 1 - 2\lambda_1)$$
$$\lambda_2(\lambda_2 - 1) = i\lambda/2$$

The third-order behavior is given by the equations

$$F(\lambda)[\lambda_1 + A_1/\lambda_1 - R_1] = A_1[A_{11}(\lambda_1 - 1) + A_{12} + A_{13} - A_{14}(\lambda_2 - \lambda_1) - A_{17}(\lambda_1^* - \lambda_1)] + \left[\frac{\theta_1}{\epsilon_1}\right]^2\left[\frac{\theta_1}{\epsilon_1}\right]^* \frac{[(\lambda_1 - R)A_3 + A_1R_1]}{8} + \left[\left(\frac{\theta_1}{\epsilon_1}\right)^2 + 2\left(\frac{\theta_1}{\epsilon_1}\right)\left(\frac{\theta_1}{\epsilon_1}\right)^*\right]\frac{[(\lambda_1 - R_1)C_{12} + A_1D_{12}]}{8} + 2\left[\left(\frac{\theta_1}{\epsilon_1}\right) + \left(\frac{\theta_1}{\epsilon_1}\right)^*\right]\frac{[(\lambda_1 - R_1)C_{21} + A_1D_{21}]}{8} + \frac{[(\lambda_1 - R_1)Q_3 + A_1B_3]}{8} + \left[\left(\frac{\theta_1}{\epsilon_1}\right)\left(\frac{\overset{m}{\theta_2}}{\epsilon_1^2}\right) + \left(\frac{\theta_1}{\epsilon_1}\right)\frac{\overset{sc}{\theta_2}}{\epsilon_1^2}\right] \times \frac{[(\lambda_1 - R_1)A_2 + A_1R_2]}{2} + \left[\left(\frac{\overset{m}{\epsilon_2} + \overset{m}{\epsilon_2}^*}{\epsilon_1^2}\right) + \left(\frac{\overset{sc}{\epsilon_2}}{\epsilon_1^2}\right)\right] \times \frac{[(\lambda_1 - R_1)Q_2 + A_1B_2]}{2} + \left\{\left(\frac{\theta_1}{\epsilon_1}\right)\left(\frac{\overset{m}{\epsilon_2} + \overset{m}{\epsilon_2}^*}{\epsilon_1^2}\right) + \left(\frac{\theta_1}{\epsilon_1}\right)\left(\frac{\overset{sc}{\epsilon_2}}{\epsilon_1^2}\right) + \left(\frac{\overset{m}{\theta_2} + \overset{m}{\theta_2}}{\epsilon_1^2}\right) + \left(\frac{\overset{sc}{\theta_2}}{\epsilon_1^2}\right)\right\} \times \frac{[(\lambda_1 - R_1)C_{11} + A_1D_{11}]}{2} + \left(\frac{\epsilon_3}{\epsilon_1^3}\right)[(\lambda_1 - R_1)Q_1 + A_1B_1] \tag{A8}$$

where

$$A_{13}\lambda_1(\lambda_1 - 1) = -(\mu_1/\epsilon_1)[K_5 + K_5^*]/2 \tag{A9}$$

$$A_{11}\lambda_1(\lambda_1 - 1) = \frac{(\mu_1/\epsilon_1)[K_5 + K_5^*]}{2\lambda_1(\lambda_1 - 1)} + \left(\frac{\mu_1}{\epsilon_1}\right) \times \frac{[(\overset{m}{\mu_2}/\epsilon_1^2) + (\overset{m}{\mu_2}/\epsilon_1^2)^*]}{4\lambda_1(\lambda_1 - 1)} - \left(\frac{\mu_1}{\epsilon_1}\right)^* \frac{(\overset{s}{\mu_2}/\epsilon_1^2)}{4\lambda_1(\lambda_1 - 1)} + \left(\frac{\mu_1}{\epsilon_1}\right) \times \left\{\frac{(K_5 + K_5^*) + (K_6 + K_6^*) - [\overset{m}{\theta_2}/\epsilon_1^2) + \overset{m}{(\theta_2}/\epsilon_1^2)^*]}{2}\right\} - \left(\frac{\mu_1}{\epsilon_1}\right)^* \frac{A_{23}}{2} \tag{A10}$$

$$A_{12}(2\lambda_1 - 1) = -\left(\frac{\theta_1}{\epsilon_1}\right)\frac{\lambda_1[\lambda_1(\lambda_1 - 1) + D](\overset{m}{\mu_2}/\epsilon_1^2) + (\overset{m}{\mu_2}/\epsilon_1^2)^*}{4\lambda_1(\lambda_1 - 1)} \tag{A11}$$

$$A_{14}\lambda_1(\lambda_1 - 1) = \left(\frac{\mu_1}{\epsilon_1}\right)^* \frac{[\overset{sc}{(\theta_2}/\epsilon_1^2) - A_{23} - A_4]\lambda_2}{2} \tag{A12}$$

$$A_{17}\lambda_2(\lambda_2 - 1) = \left(\frac{\mu_1}{\epsilon_1}\right)K_6^*\lambda_1^* + \left(\frac{\theta_1}{\epsilon_1}\right)^* \frac{\lambda_1^*[\lambda_1^*(\lambda_1^* - 1) + D^*]}{4\lambda_1^*(\lambda_1^* - 1)}\left[\frac{\overset{sc}{\mu_2}}{\epsilon_1^2}\right] \tag{A13}$$

$$A_{23}\lambda_2(\lambda_2 - 1) = \frac{(\mu_1/\epsilon_1)^2}{2\lambda_1(\lambda_1 - 1)} - \left(\frac{\overset{sc}{\mu_2}}{\epsilon_1^2}\right) \tag{A14}$$

$$A_4 = -\left(\frac{\mu_1}{\epsilon_1}\right)\left(\frac{\theta_1}{\epsilon_1}\right)\frac{\lambda_1[\lambda_1(\lambda_1 - 1) + D]}{2[\lambda_1(\lambda_1 - 1)]^2} \tag{A15}$$

$$K_5 = \frac{(\mu_1/\epsilon_1)^*(\mu_1/\epsilon_1)}{2\lambda_1(\lambda_1 - 1)} - (\overset{m}{\mu_2}/\epsilon_1^2) \tag{A16}$$

$$K_6 = \frac{(\mu_1/\epsilon_1)^*(\theta_1/\epsilon_1)\lambda_1[(\lambda_1 - 1) + D]}{2[\lambda_1(\lambda_1 - 1)]^2} \tag{A17}$$

References

[1] McClure, F. T., Hart, R. W., and Bird, J. F., "Solid Propellant Rocket Motors as Acoustic Oscillators," *ARS Progress in Astronautics and Rocketry*, Vol. 1, edited by M. Summerfield, Academic Press, New York, 1960, p. 295.

[2] Krier, H. et al., "Non-Steady Burning Phenomenon of Solid Propellants," *AIAA Journal*, Vol. 3, No. 2, Feb. 1968, pp. 278–285.

[3] Denison, M. R. and Baum, E., "A Simplified Model of Unstable Burning in Solid Rocket Propellants," *ARS Journal*, Vol. 3, No. 6, March 1961, pp. 1112–1121.

[4] Marxman, G. A. and Wooldridge, C. E., "Effect of Surface Reactions on the Solid Propellant Response Function," *AIAA Journal*, Vol. 6, No. 3, June 1968, pp. 471–478.

[5] Brown, R. S., Muzzy, R. J., and Steinle, M. E., "Surface Reaction Effects on the Acoustic Response of Composite Solid Propellants," *AIAA Journal*, Vol. 6, No. 3, March 1968, pp. 479–488.

[6] Culick, F. E. C., "Calculations of the Admittance Function for a Burning Surface," presented at the 3rd ICRPG Combustion Conference, Cocoa Beach, Florida, Oct. 1966.

[7] Friedly, J. C. and Peterson, E. E., "Influence of Combustion Parameters on Instability in Solid Propellant Motors. Part I: Development of Model and Linear Analysis," *AIAA Journal*, Vol. 4, No. 9, Sept. 1966, pp. 1605–1610.

[8] Hart, R. W., Farrell, R. A., and Cantrell, R. H., "Theoretical Study of a Solid Propellant Having a Homogeneous Surface Reaction. Part I: Acoustic Response, Low and Intermediate Frequencies," *Combustion and Flame*, Vol. 10, No. 4, 1966, pp. 367–380.

[9] Beckstead, M. W. and Culick, F. E. C., "A Comparison of Analysis and Experiment for Solid Propellant Combustion Instability," Rept. TP 4531, May 1968, Naval Weapons Center.

[10] Brown, R. S. and Muzzy, R. J., "Acoustic Response of Composite Propellants," presented at 4th ICRPG Combustion Conference, Palo Alto, October 1967.

[11] Culick, F. E. C., "A Review of Calculations for Unsteady Burning of a Solid Propellant," *AIAA Journal*, Vol. 6, No. 12, Dec. 1968, pp. 2241–2254.

[12] Friedly, J. C. and Peterson, E. E., "Influence of Combustion Parameters on Instability in Solid Propellant Motors. Part II: Nonlinear Analysis," *AIAA Journal*, Vol. 4, No. 11, Nov. 1966, p. 1932.

[13] Brown, R. S. and Muzzy, R. J., "Research on Combustion of Solid Propellants," Final Report, Contract DA-04-200-AMC-968(X), Oct. 1968, U. S. Army Ballistics Research Labs.

[14] Strittmater, R., Watermeier, L., and Pfaff, S., "Virtual Specific Acoustic Admittance Measurement of Burning Solid Propellant Surface by a Resonant Tube Technique." *Ninth Symposium (International) on Combustion*, Academic Press, New York, 1963, pp. 311–315.

[15] Friedly, J. C., "A Theoretical Analysis of Intermediate Frequency Instabilities During the Combustion of a Solid Propellant," Ph.D thesis, 1964, University of California, Berkeley.

[16] Oberg, C. L., "Combustion Instability. The Relation Between Acoustic and Non-Acoustic Instability," *AIAA Journal*, Vol. 6, No. 2, June 1968, pp. 265–271.

[17] Horton, M. D. and Rice, D. H., "The Effects of Composition of Solid Rocket Propellants," *Combustion and Flame*, Vol. 8, No. 1, 1964, pp. 21–28.

[18] Beckstead, M. W., Ryan, N. W., and Baer, A. D., "Non-Acoustic Instability of Composite Propellant Combustion," *AIAA Journal*, Vol. 4, No. 9, April 1966, pp. 1622–1628; also Beackstead, M. W. and Price, E. W., "Non-Acoustic Combustor Instability," *AIAA Journal*, Vol. 5, No. 9, 1967, pp. 1966–1989.

[19] Eisel, J. L., "The Effect of Acoustic Pressure on the Burning Rate of Solid Rocket Propellants," *Pyrodynamics*, Vol. 1, No. 2, 1964, pp. 61–70.